

Spontaneous Crystallization And Filamentation Of Solitons In Dipolar Condensates

Kazimierz Łakomy,¹ Rejish Nath,^{2,3} and Luis Santos¹

¹*Institut für Theoretische Physik, Leibniz Universität,
Hannover, Appelstrasse 2, D-30167, Hannover, Germany*

²*Max Planck Institute for the Physics of Complex Systems,
Nöthnitzer Strasse 38, D-01187 Dresden, Germany*

³*IQOQI and Institute for Theoretical Physics, University of Innsbruck, A-6020 Innsbruck, Austria*

(Dated: July 19, 2021)

Inter-site interactions play a crucial role in polar gases in optical lattices even in the absence of hopping. We show that due to these long-range interactions a destabilized stack of quasi-one dimensional Bose-Einstein condensates develops a correlated modulational instability in the non-overlapping sites. Interestingly, this density pattern may evolve spontaneously into soliton filaments or into a checkerboard soliton crystal that can be so created for the first time in ultra-cold gases. These self-assembled structures may be observed under realistic conditions within current experimental feasibilities.

PACS numbers: 03.75.Lm, 03.75.Kk, 05.30.Jp

I. INTRODUCTION

Recent experiments are opening new avenues for the study of the fascinating physics of dipolar gases [1, 2]. These gases present a significant electric or magnetic dipole-dipole interactions, which being long-range and anisotropic differ significantly from the short-range isotropic interactions usually dominant in quantum gases. Ultra-cold polar gases in optical lattices are particularly interesting. Contrary to the non-dipolar case, polar lattice gases are characterized by significant non-local inter-site interactions that result in a rich variety of novel physical phenomena [2, 3]. Remarkably, the inter-site interactions play a crucial role even in deep lattices where hopping is negligible. In particular, dipolar Bose-Einstein condensates (BECs) in non-overlapping lattice sites share common excitations modes. This collective character enhances roton-like features in the excitation spectrum [4] and modifies the BEC stability, as recently shown experimentally [5].

Quasi-1D geometries allow for the existence of BEC solitons and hence modulational instability in these systems leads to the formation of 1D patterns, so-called soliton trains [6]. On the contrary, dynamical instability in higher-dimensional BECs is typically followed by condensate collapse [7]. In consequence, solitons patterns in higher dimensions, as e.g. a 2D crystal of solitons, are fundamentally prevented in non-polar BECs.

In this paper we show that the destabilization of a dipolar BEC confined in a stack of non-overlapping quasi-1D tubes may be followed by the spontaneous self-assembly of stable soliton filaments or a 2D checkerboard crystal of solitons, providing a route for the first realization of self-sustained 2D arrangements of BEC solitons. This dynamical self-assembly stems from the correlated character of the corresponding modulational instability. While for non-dipolar condensates the instability in each lattice site would develop independently, the non-local dipolar interactions couple the non-overlapping BECs to

form a density pattern shared among all sites. As we show, correlated modulational instability may be observable in current Chromium [8] and Dysprosium [9] experiments.

The dynamically formed soliton filaments resemble dipolar chains of classical dipoles [10], as well as chains predicted for polar molecules [11, 12]. However, compared to the latter, soliton filamentation is expected to occur for smaller dipole moments due to the many-body character of each soliton. Remarkably, inverting the sign of the dipolar interactions results in the development of an anti-correlated density pattern which may be followed by the spontaneous formation of a stable crystal of solitons. This 2D checkerboard crystal resembles the Wigner-like crystal predicted for polar molecules [13, 14]. However, contrary to the latter, it is dynamically formed and self-maintained by a non-trivial interplay between intra-tube attractive and inter-tube repulsive dipolar interactions.

II. MODEL

We study below a dipolar BEC confined in a stack of quasi-1D tubes formed by an optical lattice (Fig. 1). The lattice is assumed to be sufficiently deep to suppress inter-site hopping. In each of the N_m lattice sites the xy -confinement is approximated by a harmonic potential with frequency ω_\perp , whereas for simplicity we assume no confinement along z direction. We consider atoms with a magnetic dipole moment μ (the results are equally valid for electric dipoles, as e.g. polar molecules) oriented along y direction by an external magnetic field. The dipoles interact with each other via the dipole-dipole potential $V_d(\mathbf{r} - \mathbf{r}') = g_d(1 - 3\cos^2\theta) / |\mathbf{r} - \mathbf{r}'|^3$, where $g_d = \mu_0\mu^2/4\pi$, with μ_0 being the vacuum permeability and θ the angle formed by the vector joining the two interacting particles and the dipole moment direction.

We assume the chemical potential much smaller than

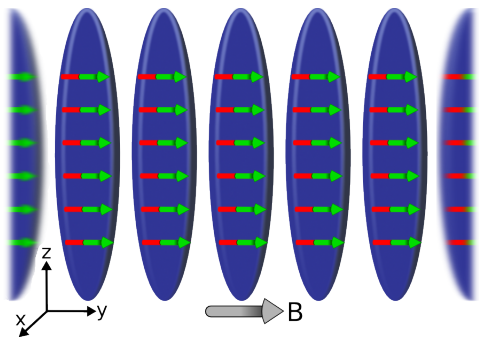


FIG. 1. (Color online) Scheme of the stack of disjoint quasi-1D dipolar BECs.

$\hbar\omega_{\perp}$ (this assumption is self-consistently verified in our calculations). Hence, we can factorize the BEC wave function at each site j , $\Psi_j(\mathbf{r}) = \phi_j(x, y)\psi_j(z)$, with $\phi_j(x, y)$ the ground-state wave function of the xy harmonic oscillator. Treating the dipolar potential in the Fourier space [15] we arrive at a system of N_m coupled 1D Gross-Pitaevskii equations describing the BEC stack:

$$i\hbar\partial_t\psi_j(z) = \left[-\frac{\hbar^2}{2m}\partial_z^2 + \frac{g}{2\pi l_{\perp}^2}|\psi_j(z)|^2 + \frac{g_d}{3}\sum_{m=0}^{N_m-1}\int\frac{dk_z}{2\pi}e^{ik_z z}\hat{n}_m(k_z)F_{mj}(k_z) \right]\psi_j(z), \quad (1)$$

where $\hat{n}_m(k_z)$ is the Fourier transform of the axial density $n_m(z)$ at site m ,

$$F_{mj}(k_z) = \int\frac{dk_x dk_y}{\pi}\left(\frac{3k_y^2}{k_x^2 + k_y^2 + k_z^2} - 1\right) \times e^{-\frac{1}{2}(k_x^2 + k_y^2)l_{\perp}^2 - ik_y(m-j)\Delta}, \quad (2)$$

$l_{\perp} = \sqrt{\hbar/m\omega_{\perp}}$ is the xy oscillator length, Δ is the lattice spacing, and $g = 4\pi a\hbar^2/m$. Note that for a fixed ratio Δ/l_{\perp} the physics of the system is governed by the values of g and g_d .

III. LINEAR REGIME: BOGOLIUBOV MODES

Starting from a homogeneous on-site linear density n_0 we are interested in the dynamics that follows the destabilization of the condensate after an abrupt change of the scattering length a . A substantial insight into the first stages of the post-instability dynamics is provided by the analysis of the elementary excitations of the condensate. To this end we introduce a perturbation of the homogeneous solution, $\psi_j(z, t) = [\sqrt{n_0} + \chi_j(z, t)]e^{-i\mu_j t/\hbar}$, with $\chi_j(z, t) = u_j e^{i(zq - \omega t)} + v_j^* e^{-i(zq - \omega t)}$, where μ_j is the chemical potential in a site j , and q and ω are the z -momentum and the frequency of the elementary excitations, respectively. Employing this ansatz in Eq.(1) we

arrive at the corresponding Bogoliubov-de Gennes equations yielding the excitation spectrum and the Bogoliubov coefficients u_j and v_j . Interestingly, even in absence of hopping, dipolar inter-site interactions result in a collective character of the excitations that are shared by all sites. In consequence, the excitation spectrum acquires a band-like character [4] as depicted in Fig. 2.

Modes with imaginary frequency are associated with dynamical instability. For non-dipolar gases, inter-site interactions are negligible and hence all transverse modes remain degenerated. As a result, modulational instability develops independently in each site and no correlated density pattern occurs during the post-instability dynamics. The situation dramatically changes for sufficiently large dipole moment, as the inter-site interactions lift the degeneracy between the transverse modes. In particular, the most unstable mode becomes significantly more unstable than other modes, as shown in Fig. 2, governing the BEC dynamics within the linear regime. Crucially, this most unstable mode is not only characterized by a z -momentum q_c (associated with the minimum of ω^2 in Fig. 2) setting the modulational instability in each wire, but also by a transverse dependence along the y direction locking the density pattern between sites. As a result, during the first stages of the post-instability dynamics a correlated modulational instability develops. Interestingly, our numerical simulations predict that this phenomenon may be observed in existing Chromium experiments [16] or even more pronouncedly with recently condensed Dysprosium atoms [9].

Fig. 3 (top) depicts the case of a ^{52}Cr BEC destabilized by an abrupt change of $a > 0$ into a sufficient $a < 0$ by means of a Feshbach resonance. The numerical solution of Eq. (1) shows that despite the absence of inter-site hopping a correlated density pattern develops. As presented in Fig. 3 (top) this instability pattern survives well into the non-linear regime where the density modulation cannot be considered any more as a perturbation of the original homogeneous on-site BECs.

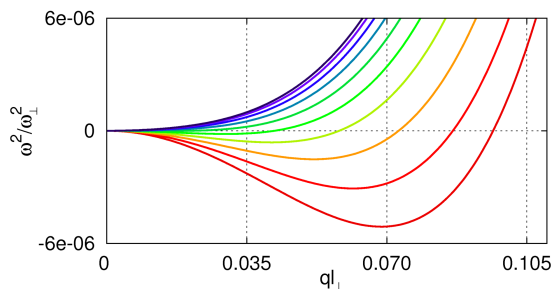


FIG. 2. (Color online) Bogoliubov spectrum for a ^{52}Cr BEC ($\mu = 6\mu_B$, where μ_B is the Bohr magneton) with a density 10^{14} cm^{-3} and $a = -8.5a_0$ (a_0 is the Bohr radius), occupying $N_m = 10$ sites of a lattice with the inter-site spacing $\Delta = 512\text{ nm}$ and a lattice depth of $13.3E_R$ (recoil energy), which results in the $\omega_{\perp} = 2\pi \cdot 26.7\text{ kHz}$, and $l_{\perp} = 85.3\text{ nm}$. Here, $q_c = 0.07/l_{\perp}$.

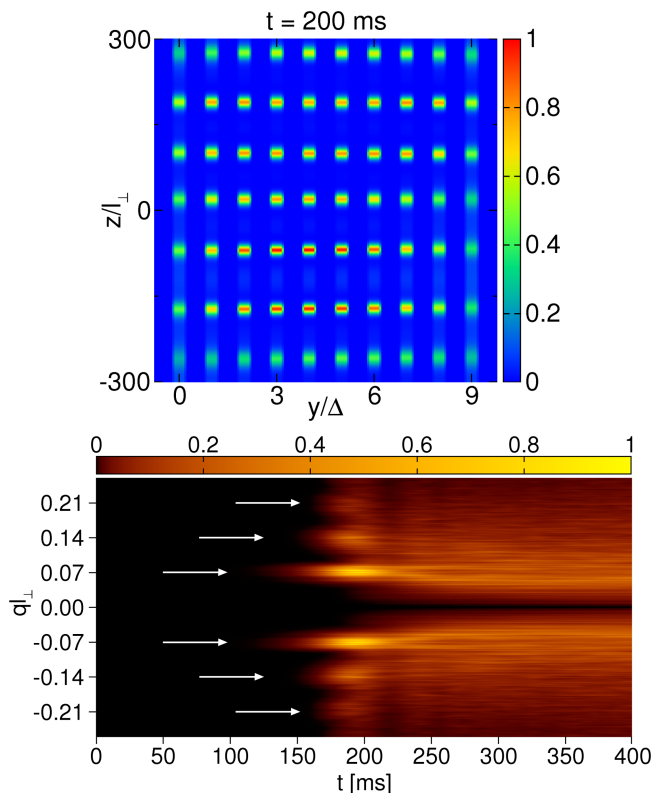


FIG. 3. (Color online) (top) BEC wave function's density distribution after 200 ms of time evolution for the same parameters as in Fig. 2. For plotting purposes the y -width of the tubes has been magnified. (bottom) Dynamics of the Fourier transform of the associated column density $\Sigma(z, t)$. The dominating $q = 0$ peak has been removed for clarity and the remaining distribution has been normalized to the maximum. The arrows indicate the harmonics of q_c .

In typical experiments the density alignments may be more easily monitored investigating the column density $\Sigma(z) = \sum_m n_m(z)$. Contrary to the uncorrelated case, for which $\Sigma(z)$ would show no clear structure, the correlated instability results in periodically modulated $\Sigma(z)$. Fig. 3 (bottom) shows the dynamics of the Fourier transform of $\Sigma(z, t)$ which is clearly characterized by the appearance of harmonics of q_c (compare Fig. 2 and Fig. 3 (bottom)).

IV. FILAMENTATION

The density modulation depicted in Fig. 3 (top) evolves into a correlated pattern of solitons. However, the solitons are created in an excited state, with both internal breathing excitation and center-of-mass motion. As a result, for insufficient dipolar interactions the correlated density modulation is destroyed during the subsequent non-linear time evolution. Consequently, the positions of solitons at different sites become uncorrelated, not differ-

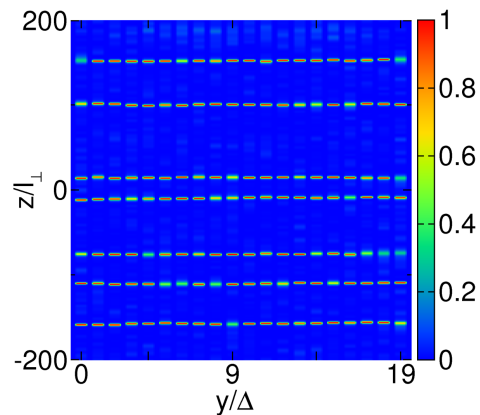


FIG. 4. (Color online) Filamentation of solitons. Here, a snapshot of time evolution of the BEC density distribution after 500 ms for, in particular, $N_m = 20$ lattice sites, $\mu = 18\mu_B$ and $a = -41.7a_0$. The remaining parameters are chosen as in the case of Fig. 2.

ing qualitatively from the case of non-polar gases. Strong inter-site interactions crucially change this picture as the correlated solitons in neighboring sites experience an attractive inter-site potential. Approximating the solitons by Gaussians of width δ , such that $l_{\perp} \ll \delta, \Delta$, the binding energy for two solitons acquires the form

$$E_b = (-2g_d/\Delta^3)G(\delta/\Delta), \quad (3)$$

which differs from the binding energy between point-like solitons $(-2g_d/\Delta^3)$ by the regularization function

$$G(x) \simeq \frac{e^{1/4x^2}}{4\sqrt{2\pi}x^3} \left[(x^2+1)K_0\left(\frac{1}{4x^2}\right) + (x^2-1)K_1\left(\frac{1}{4x^2}\right) \right] \quad (4)$$

with K_n the modified Bessel function of second kind. As a result of this inter-site soliton attraction, and although the initial periodicity of the modulation (as that of Fig. 3 (top)) is generally lost, self-assembled soliton filaments form spontaneously (Fig. 4) when the center-of-mass kinetic energy of the solitons acquired in the post-instability dynamics cannot overcome the binding energy given by Eq. (3).

In order to analyze the dynamical filamentation quantitatively we introduce at this point the time-dependent dimer correlation function for sites m and m'

$$G_{m,m'}(z, t) = \int dz' n_m(z', t) n_{m'}(z' + z, t) \quad (5)$$

and we define the normalized average dimer correlation $G^n(z, t) = G(z, t)/\int dz G(z, t)$, with

$$G(z, t) = \frac{2}{N_m(N_m-1)} \sum_m \sum_{m'>m} G_{m,m'}(z, t). \quad (6)$$

A proper figure of merit describing the filamentation is provided by

$$\chi(t) = G^n(0, t)/\bar{G}^n(t), \quad (7)$$

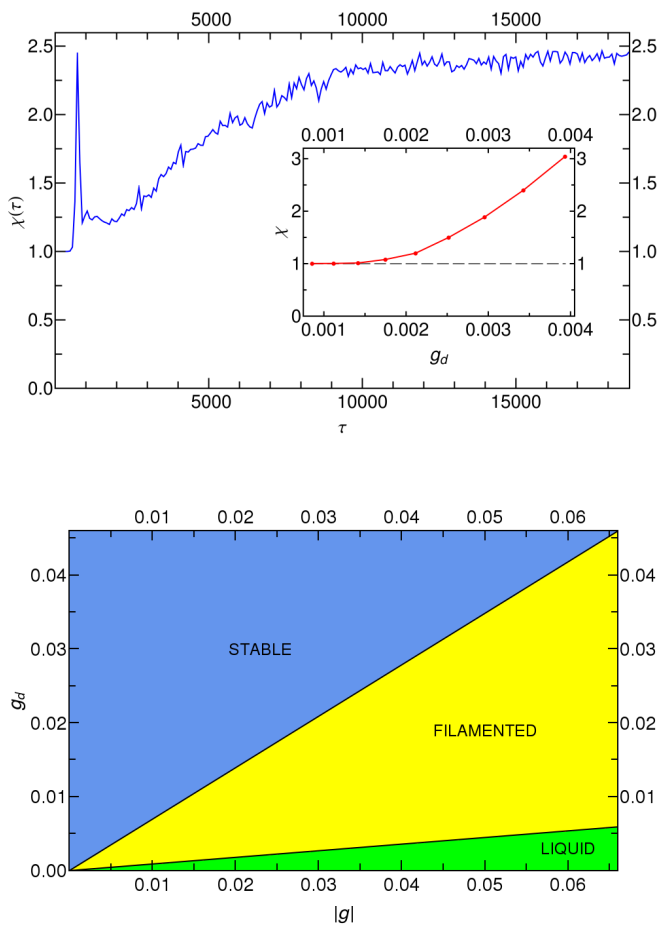


FIG. 5. (Color online) (top) Function $\chi(\tau)$ for a typical case within the filamentation regime ($g = -0.019$, $g_d = 0.0034$, $\Delta = 6l_\perp$). In particular, for the parameters that we employed in Fig. 2 the time ($t = \tau/\omega_\perp$) that we here consider equals $t = 700$ ms. (inset) Time-averaged values of χ for long times, for different values of g_d and constant $g = -0.019$. (bottom) Phase diagram of the possible regimes for $g < 0$, $g_d > 0$.

where $\bar{G}^n(t) = \int dz G^n(z, t)^2$ is the mean value of $G^n(z, t)$. Such defined function $\chi(t)$ characterizes the tendency of the solitons at different sites to align into a filament.

In the following analysis we consider a simplified case of three lattice sites. Fig. 5 (top) shows $\chi(t)$ for a typical case within the filamentation regime (see discussion below). The sharp initial peak indicates the formation of the correlated density pattern shared among all sites at the initial stage of the time evolution, as discussed in section III. Similarly to Fig. 3, also here the pattern is quickly destroyed as the system enters the non-linear regime. However, provided sufficiently strong dipolar interactions, the inter-site soliton binding E_b supports the formation of soliton filaments and in consequence $\chi(t)$ grows at larger times. Note that $\chi(t)$ eventually saturates remaining constant for times typically much longer than the usual experimental timescales.

In contrast, no filamentation occurs if the dipolar cou-

pling is insufficient. In this case, at long times $\chi(t)$ averages to $\chi = 1$ indicating the absence of inter-site soliton-soliton correlation. Hence, driving the g_d parameter from small to large values results in a transition from a non-filamented into a filamented configuration (see the inset of Fig. 5 (top)). Ultimately, for a sufficiently large g_d the repulsive on-site interactions compensate the attractive short-range interactions and the system remains stable.

As a result, we distinguish three distinct regimes of dynamics in a stack of 1D dipolar gases: (i) unstable uncorrelated (soliton liquid), (ii) unstable filamented, and (iii) stable. As shown in Fig. 5 (bottom), for a fixed value of Δ/l_\perp these regimes are determined by the ratio $g_d/|g|$. For the considered case of three sites and $\Delta/l_\perp = 6$ the stability boundary line is given by $g_d/|g| = 0.70$, whereas the boundary line between the filamented and unstable non-filamented regimes occurs at $g_d/|g| = 0.09$. For the case of ^{52}Cr ($\mu = 6\mu_B$) the filamentation occurs for $5.2 < |a|/a_0 < 40.2$, whereas for ^{164}Dy ($\mu = 10\mu_B$) it occurs for $47.3 < |a|/a_0 < 367.0$.

We note that for a larger number of sites the system is more unstable due to the inter-site attractive interactions [4]. Also, the boundary between filamented and unstable non-filamented regimes is shifted towards larger g_d values due to the enhanced role of the string-like modes of the filaments. Hence, even though the qualitative results will not be affected, increasing the number of sites will in general reduce the filamentation regime.

V. CHECKERBOARD SOLITON CRYSTAL

Interestingly, the sign of g_d may be inverted by means of transverse magnetic fields [17] or microwave dressing in the case of polar molecules [18]. Note that, although we consider this case for its theoretical simplicity, qualitatively the same results may be obtained orienting the dipoles along the tubes. In both of these cases the emerging instability is characterized by the most unstable Bogoliubov mode presenting a staggered y -dependence that results in an anti-correlated density pattern with maxima in a given site aligned with minima in the neighboring ones. Strikingly, for a sufficiently strong dipole moment, this anti-correlated structure formed at the initial stage of the post-instability dynamics seeds the formation of a permanent checkerboard soliton crystal in the non-linear regime, as shown in Fig. 6.

Remarkably, while purely repulsive interactions sustain 2D Wigner-like crystals proposed for polar molecules [13, 14], the crystal of solitons is self-maintained by a subtle interplay of dipolar inter-tube repulsion and intra-tube attraction. Due to the anti-correlated character of the density modulation, solitons in neighboring sites provide an effective potential barrier that prevents mutually attracting solitons in the same tube to come together, hence keeping the crystal stable.

In order to characterize quantitatively the dynamical formation of a soliton crystal, we employ the

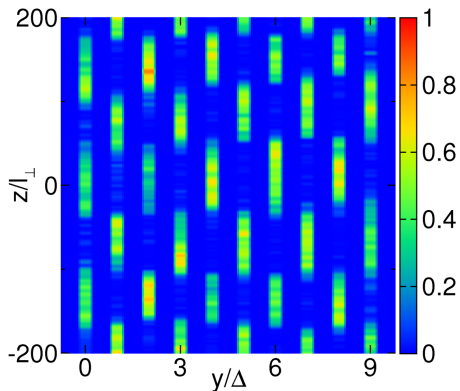


FIG. 6. (Color online) Spontaneous crystallization of solitons in the case of negative g_d . Here, $a = 306a_0$, $\mu = 36\mu_B$ and the remaining parameters such as in Fig. 2.

notation introduced in section IV, defining the normalized averaged nearest-neighbor (NN) and next-to-nearest-neighbor (NNN) dimer correlations $G_\alpha^n(z, t) = G_\alpha(z, t) / \int dz G_\alpha(z, t)$, with $\alpha = NN, NNN$ and

$$G_{NN}(z, t) = \frac{1}{N_m - 1} \sum_m G_{m, m+1}(z, t), \quad (8)$$

$$G_{NNN}(z, t) = \frac{1}{N_m - 2} \sum_m G_{m, m+2}(z, t), \quad (9)$$

and we introduce functions

$$\chi_\alpha(t) = G_\alpha^n(0, t) / \bar{G}_\alpha^n(t) \quad (10)$$

where $\bar{G}_\alpha^n(t) = \int dz G_\alpha^n(z, t)^2$ is the mean value of $G_\alpha^n(z, t)$. The checkerboard soliton arrangement is characterized by the NN anti-correlation ($\chi_{NN}(t) < 1$) and the NNN correlation ($\chi_{NNN}(t) > 1$). In the following we consider a particular case of four lattice sites. A generic example of $\chi_{NN}(t)$ and $\chi_{NNN}(t)$ time evolution within the crystalline regime (see discussion below) is depicted in the inset of Fig. 7 (top).

As in the case of filamentation, the emergence of the soliton crystal is limited to a window of $|g_d|/g$ values. While for a weak dipolar coupling the system remains stable, a sufficiently large dipole moment value renders the attractive intra-tube interactions dominant and, in consequence, we observe the formation of the staggered soliton pattern. Note that this configuration, originating in the anti-correlated modulational instability emerging within the linear regime, is indeed a highly metastable state, as it maximizes NNN dipolar interactions. Crucially, however, our numerical simulations show that such soliton crystal state characterized by $\chi_{NN}(t) < 1$ coinciding with $\chi_{NNN}(t) > 1$ remains stable well beyond typical experimental timescales, being hence effectively permanent. Beyond a critical value of the dipolar coupling the NNN repulsion destroys the NNN anticorrelation and hence the crystal.

The instability properties of the soliton crystal may be studied by considering the average χ_α for different

time windows, as depicted in Fig. 7 (top). For all g_d values within the unstable regime the NN anticorrelation function $\chi_{NN}(t) < 1$ remains constant at all times. In contrast, depending on the value of the g_d parameter, $\chi_{NNN}(t)$ function shows two distinctive types of time dependence. Namely, while in the window of the crystallization regime $\chi_{NNN}(t)$ saturates at a value indicating NNN anticorrelation and so the emergence of a stable soliton crystal. Contrastingly, for large dipolar interactions the initially anticorrelated χ_{NNN} , which originates in the linear regime, decreases in time indicating destruction of the checkerboard pattern.

Hence, for negative g_d values we identify three distinct regimes depicted in Fig. 7 (bottom): (i) a stable regime for small dipole values, (ii) an unstable regime intrinsically characterized by the dynamical formation of a checkerboard soliton crystal, and (iii) a strong dipolar

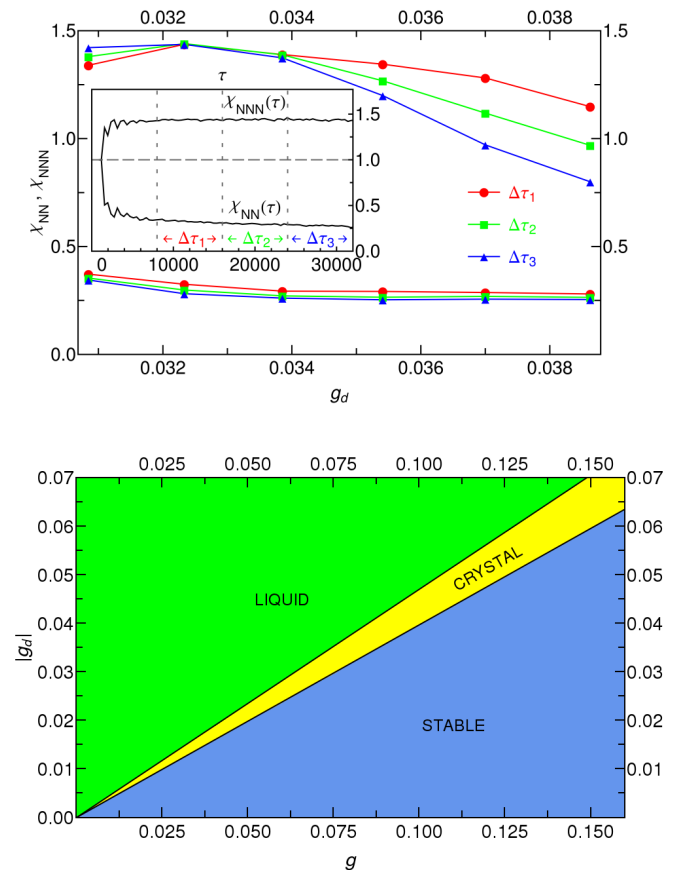


FIG. 7. (Color online) (top) The inset shows a typical example of time evolution of $\chi_{NN}(\tau)$ and $\chi_{NNN}(\tau)$ within the soliton crystal regime ($g = 0.069$, $g_d = -0.032$ and $\Delta = 6l_\perp$). We average $\chi_\alpha(\tau)$ within three different time intervals $\Delta\tau_{1,2,3}$, and we depict in the figure the corresponding averaged χ_α (\bullet , \blacksquare , \blacktriangle) for different values of g_d and constant $g = 0.069$. Note that for $|g_d|/g > 0.47$, χ_{NNN} decreases in time, indicating destruction of the checkerboard crystal. In particular, for the parameters we employed in Fig. 2, the time ($t = \tau/\omega_\perp$) that we here consider equals $t = 1200$ ms. (bottom) Phase diagram of the possible regimes for $g > 0$, $g_d < 0$.

interactions regime in which only nearest neighbor anti-correlation is preserved while the next-to-nearest neighbor correlation is lost (soliton liquid). In analogy to the filamentation phenomenon, for a fixed Δ/l_{\perp} value the regimes boundaries depend solely on the $|g_d|/g$ ratio. For $\Delta/l_{\perp} = 6$, the crystallization regime occurs for $0.40 < |g_d|/g < 0.47$, which for ^{52}Cr (^{164}Dy) requires $7.7 < a/a_0 < 9.1$ ($70.0 < a/a_0 < 82.9$).

VI. SUMMARY

In conclusion, the dipolar inter-site interactions in a destabilized dipolar BEC confined in a stack of quasi-1D tubes induce an interesting dynamics characterized by the development of a correlated modulational instability in the non-overlapping sites. For a sufficiently large dipole moment this density modulation seeds the spontaneous self-assembly of soliton filaments or a soliton checkerboard crystal, depending on the sign of the

dipolar interactions. Contrary to filaments and crystals of individual molecules, filaments and crystals of solitons self-assemble spontaneously merely by simple destabilization of the condensate. Moreover, we expect that due to the many-body character of the constituent solitons the dipole moment necessary for observing these structures may be significantly reduced and that they may be attainable with partially polarized polar molecules [19] or highly magnetic atoms, paving a promising route towards the first realization of 2D patterns of solitons in ultra-cold gases and, to the best of our knowledge, in nonlinear optics as well.

ACKNOWLEDGMENTS

We acknowledge the support of the Center of Excellence QUEST, the German-Israeli Foundation and the DFG (SA1031/6).

-
- [1] M. Baranov, *Phys. Rep.* **464**, 71 (2008).
 - [2] T. Lahaye *et al.*, *Rep. Prog. Phys.* **72**, 126401 (2009).
 - [3] C. Trefzger *et al.*, *J. Phys. B* **44**, 193001 (2011).
 - [4] M. Klawunn and L. Santos, *Phys. Rev. A* **80**, 013611 (2009).
 - [5] S. Müller *et al.*, *Phys. Rev. A* **84**, 053601 (2011).
 - [6] K. E. Strecker *et al.*, *Nature* **417**, 150 (2002).
 - [7] E. A. Donley *et al.*, *Nature* **412**, 295 (2001).
 - [8] T. Lahaye *et al.*, *Nature* **448**, 672 (2007).
 - [9] M. Lu *et al.*, *Phys. Rev. Lett.* **107**, 190401 (2011).
 - [10] P. I. C. Teixeira, J. M. Tavares, and M. M. Telo da Gama, *J. Phys. Cond. Matt.* **12**, R411 (2000).
 - [11] D.-W. Wang, M. D. Lukin, and E. Demler, *Phys. Rev. Lett.* **97**, 180413 (2006).
 - [12] M. Klawunn, J. Duhme, and L. Santos, *Phys. Rev. A* **81**, 013604 (2010).
 - [13] H. P. Büchler *et al.*, *Phys. Rev. Lett.* **98**, 060404 (2007).
 - [14] G. Pupillo *et al.*, *Phys. Rev. Lett.* **100**, 050402 (2008).
 - [15] K. Góral and L. Santos, *Phys. Rev. A* **66**, 023613 (2002).
 - [16] T. Lahaye *et al.*, *Phys. Rev. Lett.* **101**, 080401 (2008).
 - [17] S. Giovanazzi, A. Görlitz, and T. Pfau, *Phys. Rev. Lett.* **89**, 130401 (2002).
 - [18] A. Micheli *et al.*, *Phys. Rev. A* **76**, 043604 (2007).
 - [19] K.-K. Ni *et al.*, *Nature* **464**, 1324 (2010).